Electronic Supplementary Information (ESI)

Aliphatic-aromatic sulphonated polyimide and acid functionalized polysilsesquioxane composite membrane for fuel cell applications

Ravi P. Pandey,[a,b] **Vinod K. Shahi**[*a,b]

[a]*Academy of Scientific and Innovative Research, INDIA*
[b]*Electro-Membrane Processes Division,*
CSIR-Central Salt & Marine Chemicals Research Institute,
G. B. Marg, Bhavnagar-364002 (Gujarat), INDIA
Tel: +91-278-2569445; Fax: +91-278-2567562/2566970; E-mail: vkshahi@csmcri.org; vinodshahi1@yahoo.com

S1. Synthesis of BAPBDS

To a 100 ml three-neck flask, equipped with a mechanical stirring device, 11.0 g (30 mmol) of BAPB was added. In cooled (ice bath) flask 18 ml of concentrated sulphuric acid was slowly added under constant stirring. The mixture was continuously stirred at 0 ^{o}C for 30 min followed by slight heating until the BAPB was dissolved. 4.2 ml of fuming sulphuric acid (60% SO_3) was slowly added to the cooled mixture and under stirring (30 min.) at 0 ^{o}C and for 2 h at 50 ^{o}C. Reaction mixture was cooled to room temperature and poured into crushed ice. Filtered off solid was dissolved in NaOH solution. Filtrate was acidified with concentrated hydrochloric acid. Precipitate was washed with de-ionized water, methanol, and dried at 90 ^{o}C in vacuum. **^{1}H NMR** spectrum (in DMSO-d6 in the presence of a drop of Et_3N for dissolution of BAPBDS): **δ (ppm) 7.96, 7.43, 6.78, 6.69, 6.60, and 4.92.**

S2. Instrumental characterization of the membranes

^{1}H NMR spectra of BAPBDS (in presence of one drop Et_3N for dissolution) and ^{1}H and ^{13}C spectra for SPI and SSP were recorded in DMSO-d_6 spectrometer (Bruker, 500 MHz). ^{29}Si NMR spectra of dried membranes were recorded in solid state using spectrometer (Bruker, 500 MHz).

Infrared (IR) spectra were obtained as KBr pellets (4000-400 cm^{-1}) using spectrum GX series 49387 spectrometer.

Thermal stability of the membranes was investigated by thermo gravimetric analyzer (TGA) (Mettler Toledo TGA/SDTA851 with Star software) under N_2 atmosphere with 10 °C/min heating rate from 30 to 800 °C. Glass transition behavior was assessed by differential scanning calorimetry (DSC) in -50–250 ◦C with 5 ◦C/min heating rate. Mechanical stability of membranes were analyzed by Mettler Toledo dynamic mechanical analyzer (DMA) 861 with Star software under N_2 atmosphere with 10 °C/min heating rate from 0 to 400 °C.

Scanning electron microscopy (SEM) was recorded by Leo microscope (Kowloon, Hong Kong) after gold sputter coatings on dried membrane samples. Energy-dispersive X-ray (EDX) study was performed by LEO VP1430 and an Oxford Instruments (Oxfordshire, UK) INCA. Transmission electronic microscopy (TEM) images of the SPI samples were recorded using a JEOL JEM 2100 microscope. The powder samples were dispersed in ethanol and mounted on a lacey carbon Formvar coated Cu grid. Atomic force microscopy (AFM) images of dried membranes were obtained by NTEGRA AURA (NTMDT) in semi-contact mode.

S3. Water uptake and water retention studies

The membrane swelling properties were obtained in terms of water uptake. For the determination of weight fraction of water, the membranes were immersed in distilled water for 24 h and the wet weight was recorded after removing surfacial water. Then the wet membranes were dried under vacuum at 60 ^{o}C until to get a constant weight and thus dry weight of the membranes were recorded. The water uptake (%) of the membranes was determined using the following equation.

$$Water\ uptake(\text{wt}\,\%) = \frac{W_{wet} - W_{dry}}{W_{dry}} \times 100 \qquad (1)$$

where W_{wet} and W_{dry} are the masses of the membrane under wet and dry conditions.

The volume fraction of water in the membrane phase (φ_w) of the membranes was determined by the following equation:

$$\varphi_w = \frac{\frac{\Delta w}{d_w}}{\frac{\Delta w}{d_w} + \frac{w_d}{d_p}} \qquad (2)$$

where Δw is the weight difference between wet and dry membrane, w_d is the weight of dry membrane and *dw* and *dp* are the densities of water and dry membrane, respectively.

The water retention ability of the developed membranes was evaluated by measuring water mobility during the dynamic deswelling test. Fully swollen membranes were placed in desiccators containing silica gel (drying agent) at 35 ^{o}C and were weighed after regular intervals. The weight of fully swollen membranes (W_{wet}), weight of membrane at time *t* (W_t), and weight of dry membrane (W_{dry}) were recorded. The deswelling profile can be obtained by plotting (M_t/M_o)-time curve using the following equation:

$$\frac{Mt}{Mo} = 4\left(\frac{D\,t}{\pi\,l^2}\right)^{1/2} \qquad (3)$$

where M_0 is the initial amount of water in membrane ($M_0 = W_{wet} - W_{dry}$), and M_t is the amount of water remaining in the membrane at any given time ($M_t = W_t - W_{dry}$), D is water diffusion coefficient, and *l* is the membrane thickness.

S4. Ion-exchange capacity (IEC) measurements

The IEC of the membranes was determined by an acid-base titration method. Before testing, the dried membrane with proton exchange groups in the form of sulphonic acid was soaked in 50 ml of a saturated NaCl solution for 48 h to liberate the H^+ ions into the solution by an ion exchange with the Na^+ ions. With the membrane kept in the solution, the release H^+ ions were then titrated

with a NaOH solution using phenolphthalein as an indicator. The value of IEC was then determine as

$$IEC(mequiv.g^{-1}dry\ membrane) = \frac{N_{NaOH} \times V_{NaOH}}{W_{dry}} \qquad (4)$$

where N_{NaOH} and V_{NaOH} are, respectively, the concentration and the consumed volume of the NaOH solution.

S5. Proton conductivity measurements

Membrane conductivity measurements were carried out in equilibration with water using a potentiostat/galvanostat frequency response analyzer (Auto Lab, Model PGSTAT30). The membranes were sandwiched between two in-house made stainless steel circular electrodes (4.0 cm^2). Direct current (DC) and sinusoidal alternating currents (AC) were supplied to the respective electrodes for recording the frequency at a scanning rate of 1μA/s within a frequency range of 10^6 to 1 Hz. The spectrum of the blank short-circuited cell was also collected and this data was subtracted (as a series circuit) from each of the recorded spectra of the membranes to eliminate cell and wiring resistances and inductances. The corrected spectra were viewed as complex impedance plots with the imaginary component of Z'' on the y-axis and the real component of Z' on the x-axis ($Z = Z'\text{-}iZ''$); the ionic resistance of each membrane was estimated to be the intersection of the x-axis with the extrapolation of the low frequency linear component of each plot. The membrane resistances were obtained from Nyquist plots. The proton conductivity (κ^m) was calculated from eq:

$$\kappa^m(S/cm) = \frac{L(cm)}{[R(\Omega) \times A(cm^2]} \qquad (5)$$

Where, L is the distance between the electrodes used to measure the potential, R is the resistance of the membrane, and A is the surface area of the membrane.

S6. Methanol permeability

Methanol permeability of the composite membrane was determined in a diaphragm diffusion cell, consisting of two compartments (80 cm^3) separated by a vertical membrane with 20 cm^2 effective area. The membrane was clamped between both compartments, which were stirred during the experiments. Before the experiment, membranes were equilibrated in water-methanol mixture for 12 h. At the beginning, one compartment (A) was filled with pure or 8M methanol, and the other compartment (B) was filled with double distilled water. Methanol flux arises across the membrane as a result of concentration difference between two compartments. The increase in methanol concentration with time in compartment B was monitored by measuring the refractive index using a digital refractometer (Mettler Toledo RE40D refractometer). The methanol permeability (P) finally was obtained by the equation given below:

$$P = \frac{1}{A}\frac{C_{B(t)}}{C_A(t-t_0)}V_B l \qquad (6)$$

Where A is the effective membrane area, l the thickness of the membrane, $C_{B(t)}$ the methanol concentration in compartment B at time t, $C_A(t\text{-}t_0)$ the change in the methanol concentration in compartment A between time 0 and t, and V_B the volume of compartment B. All experiments were carried out at room temperature, and the uncertainty of the measured values was less than 2%.

S7. Estimation of frictional coefficient between proton and membrane matrix (f_{sm})

X^m the fixed charge concentration in the membrane matrix (moles of fixed charge/volume of wet membrane), and was estimated by following equation:

$$X^m = \frac{\tau(IEC)\rho_d}{\varphi_w} \qquad (7)$$

ρ_d is the density of dry membrane, and τ was estimated by:

$$\tau = \frac{\varphi_w}{1 + \varphi_w} \qquad (8)$$

ω is the proton mobility coefficient across the membrane and was estimated by:

$$\omega = \frac{[H^+]_{est}\, \varphi_w^2\, \theta}{X^m \Delta x\, f_{2w}^0} \qquad (9)$$

Where θ denotes touristy factor (inversely proportional to the true path length of proton) and may be estimated by:

$$\theta = \frac{\kappa^m f_{1w}^0\, \Delta x}{F^2 X^m} \qquad (10)$$

f_{1w}^o and f_{2w}^o are the frictional coefficient between co-ion (OH^-) and counter-ion (H^+) and water in free solution, respectively and may be obtained as $f_{1w}^o = RT/D_i$. D_i is the diffusion coefficient of single ion "*i*" in the free solution and was obtained from ionic conductance data.

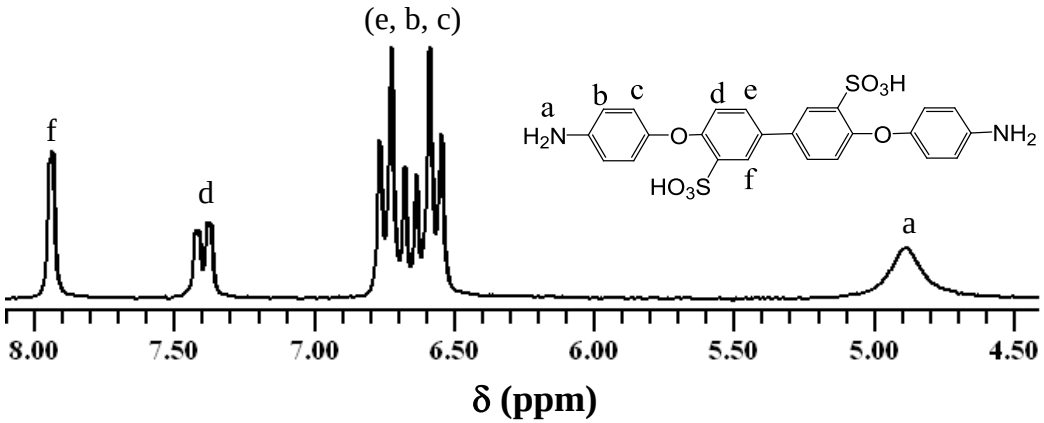

Fig. S1 ^{1}H NMR spectrum of BAPBDS in DMSO-d_6 in the presence of a drop of Et_3N for dissolution of BAPBDS.

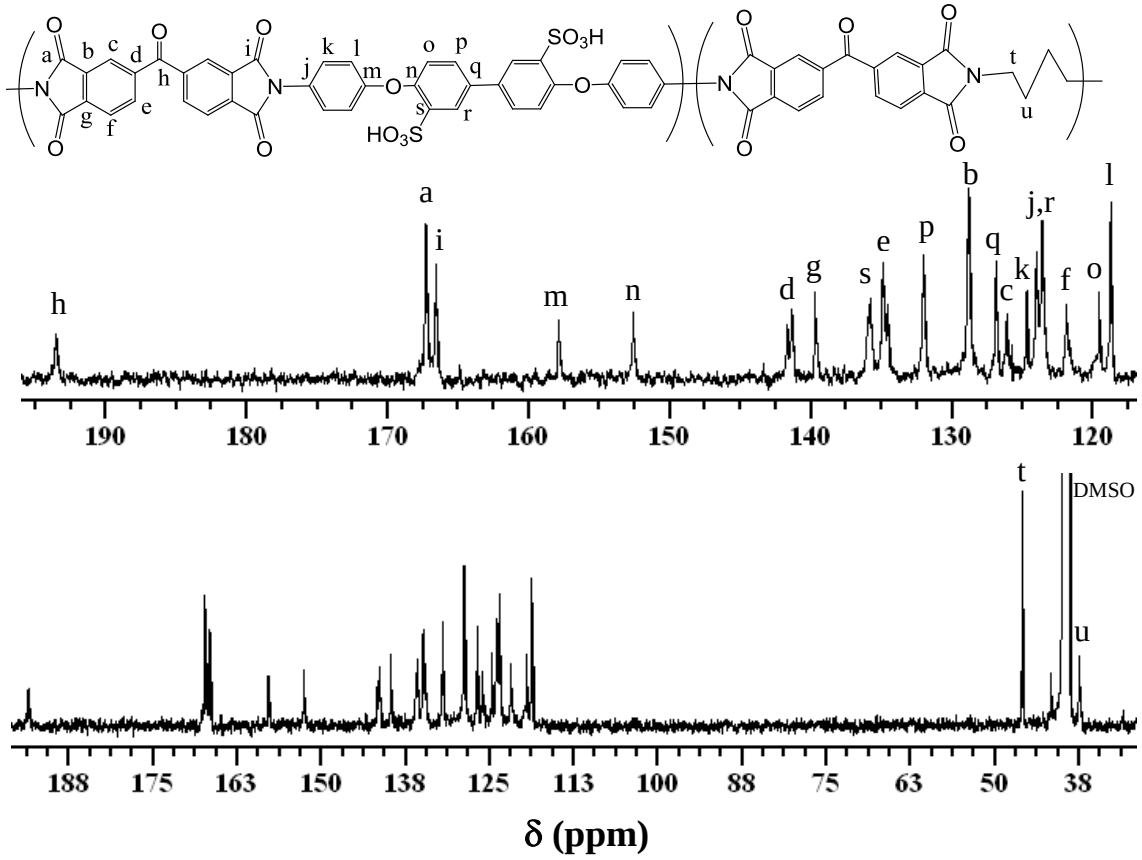

Fig. S2 ^{13}C NMR spectrum of SPI in DMSO-d_6.

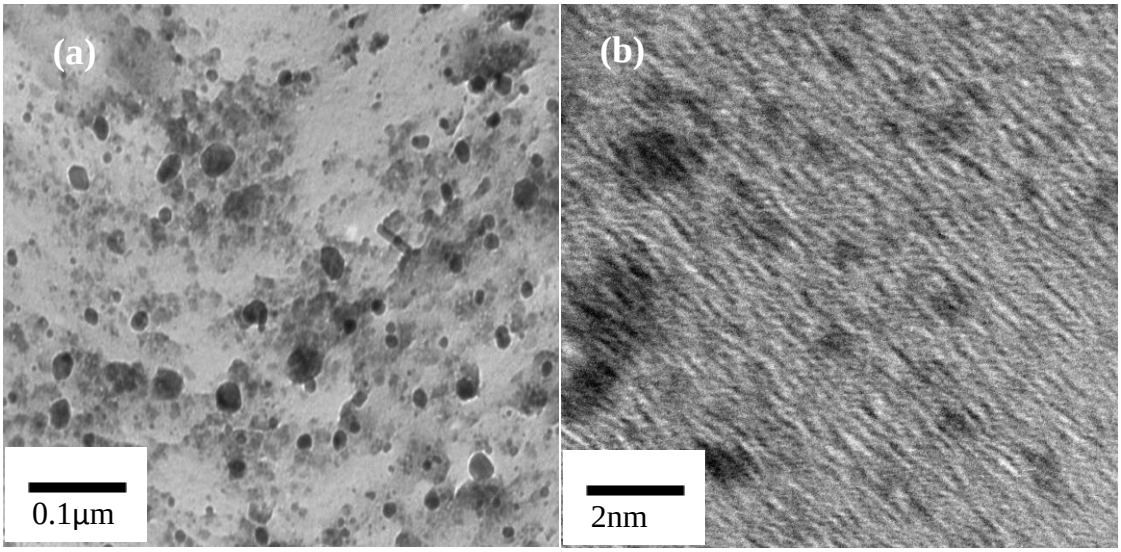

Fig. S3 TEM image of SPI (a) at low resolution and (b) at high resolution.

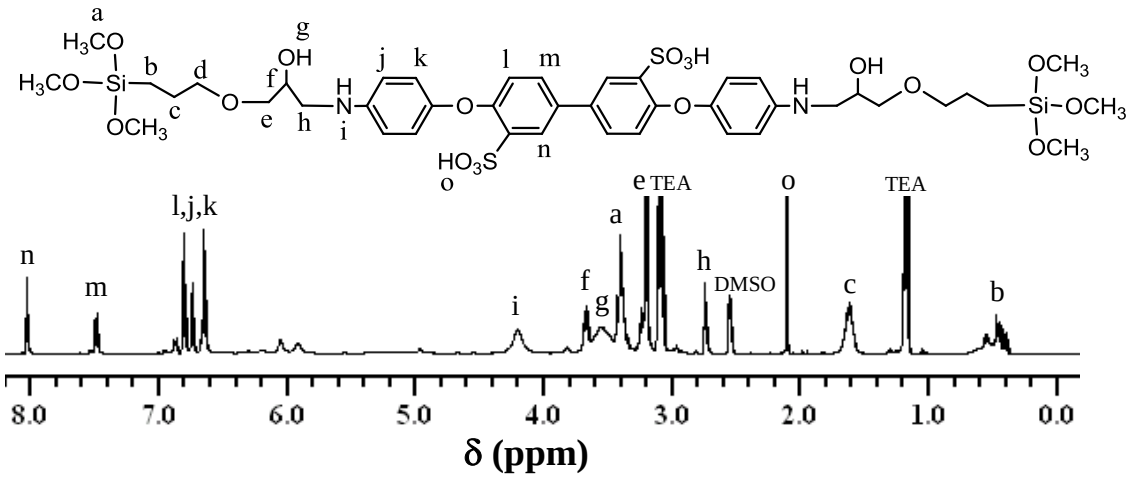

Fig. S4 ^{1}H NMR spectrum of SSP in DMSO-D_6.

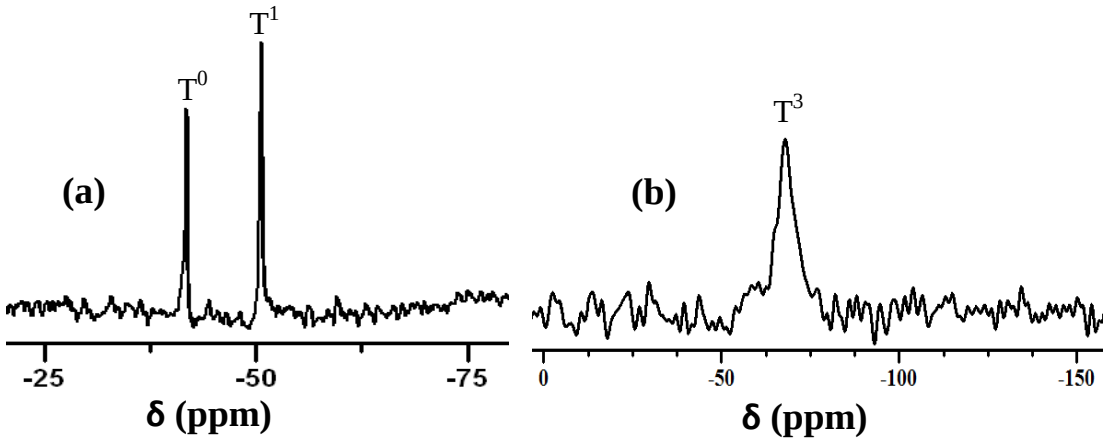

Fig. S5 ^{29}Si NMR spectra of **(a)** SSP in DMSO-d_6 and **(b)** SPI/SSP-40 composite in solid state.

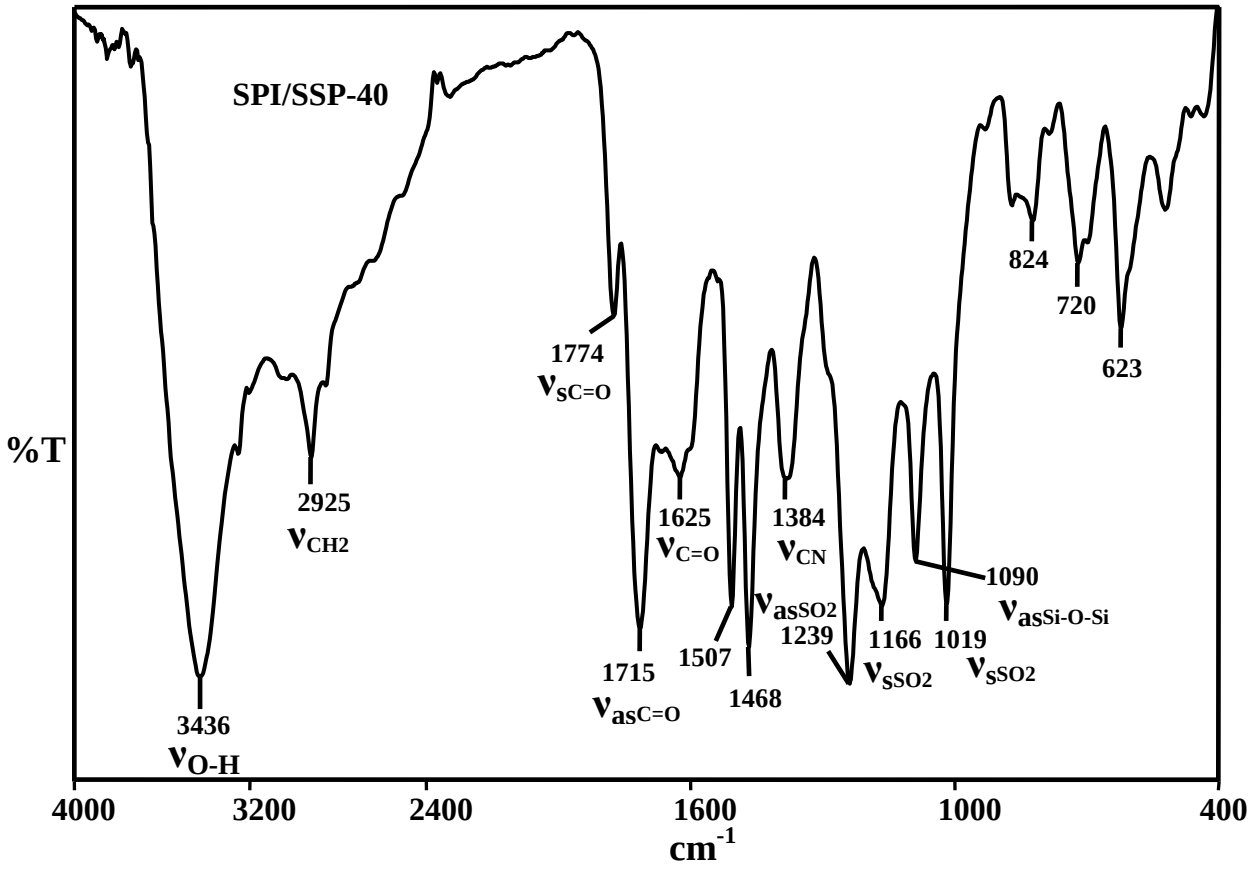

Fig. S6 FTIR spectrum of SPI/SSP-40.

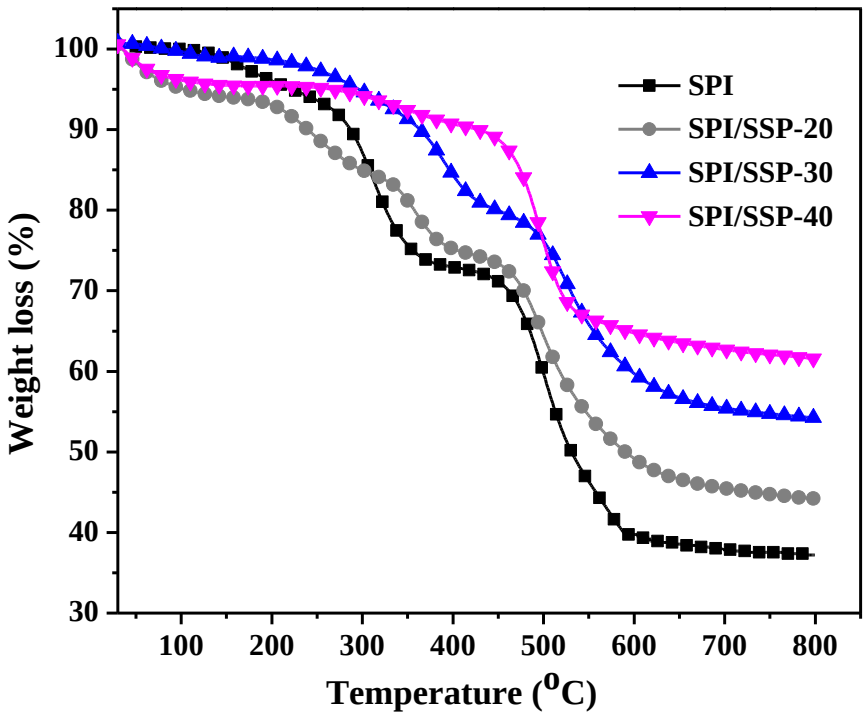

Fig. S7 TGA curves of SPI and different composite membranes.

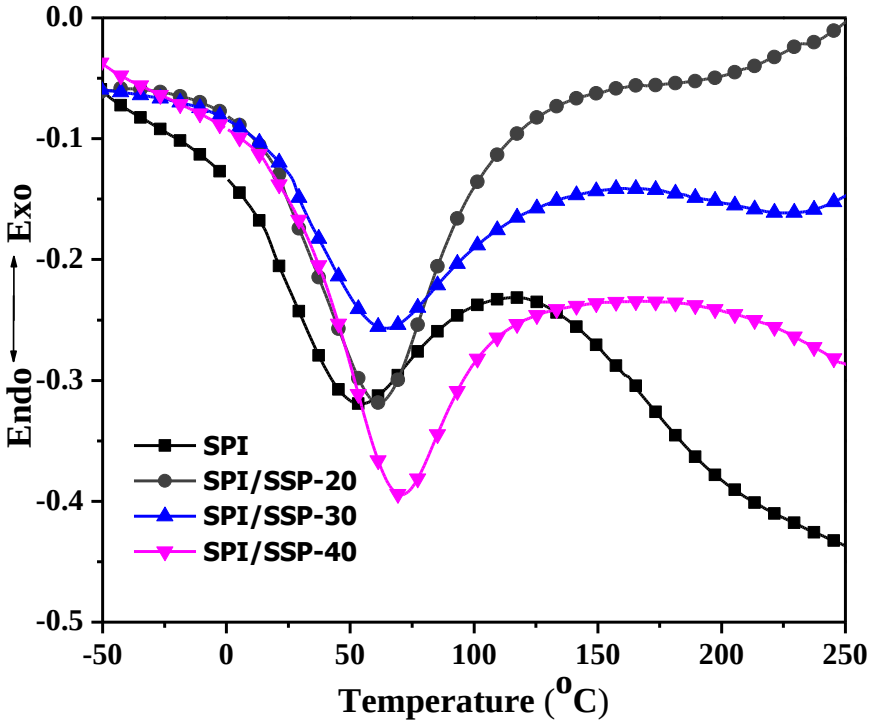

Fig. S8 DSC analysis of SPI and different composite membranes.

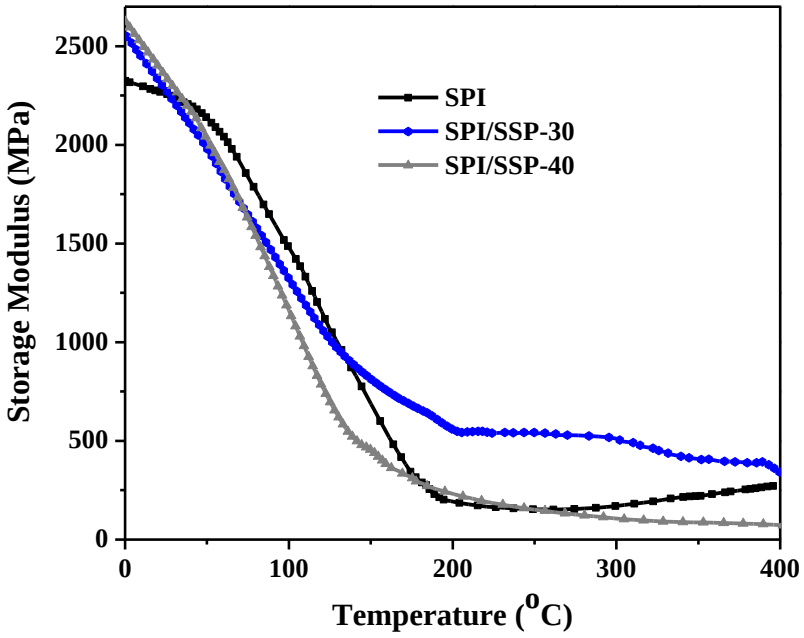

Fig. S9 DMA curves showing the effect of SSP concentration on mechanical property.

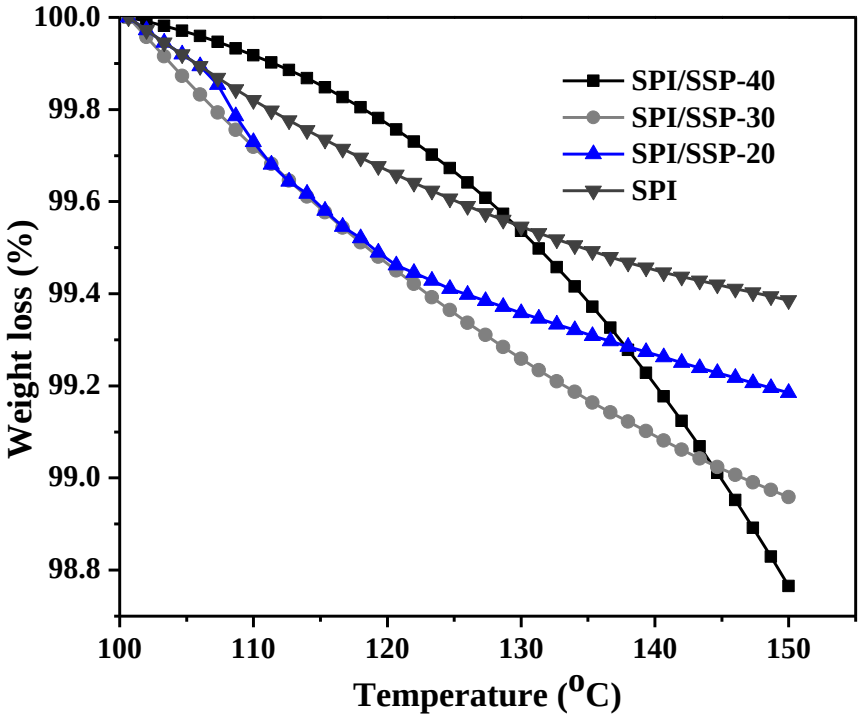

Fig. S10 The bound water content comparison of different membranes.

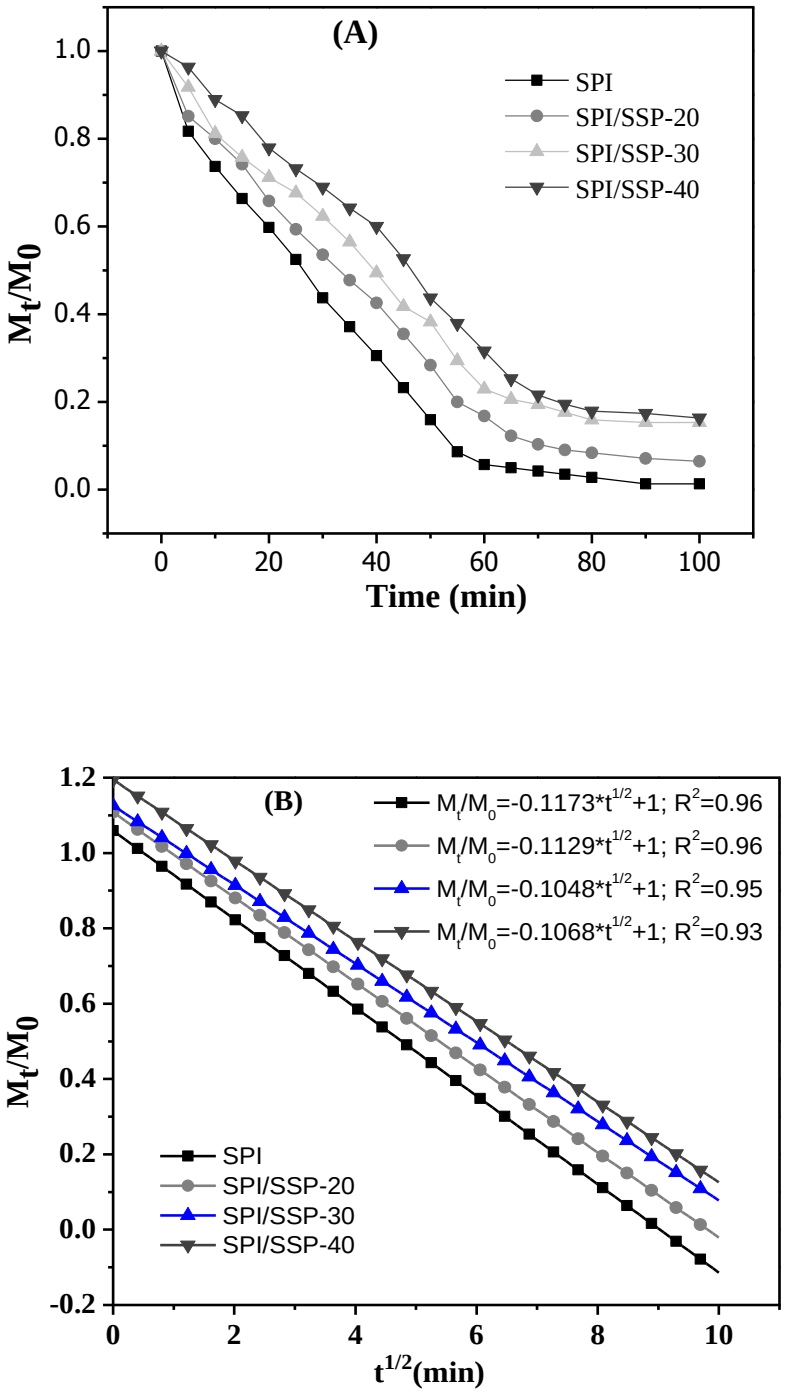

Fig. S11 Water desorption profile for SPI and composite membranes: (A) isotherm at 35^0C; (B) Higuchi's model fit of the deswelling behavior.

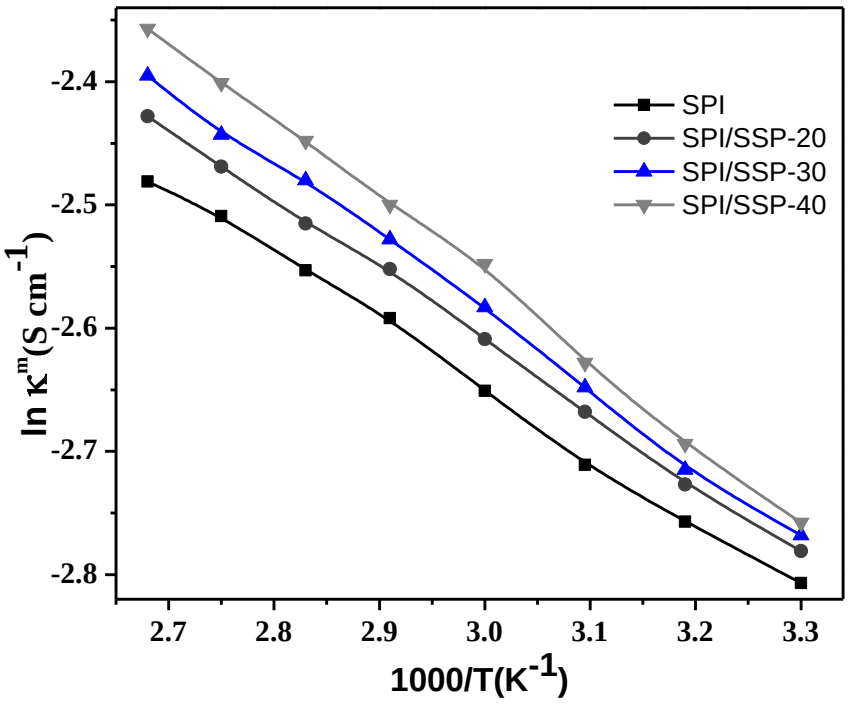

Fig. S12 Arrhenius plot in 100% RH environment, for different developed proton exchange membranes.